

Experimental measurement of oil–water two-phase flow by data fusion of electrical tomography sensors and venturi tube

This content has been downloaded from IOPscience. Please scroll down to see the full text.

2017 Meas. Sci. Technol. 28 095301

(<http://iopscience.iop.org/0957-0233/28/9/095301>)

[View the table of contents for this issue](#), or go to the [journal homepage](#) for more

Download details:

IP Address: 58.60.1.3

This content was downloaded on 19/08/2017 at 13:49

Please note that [terms and conditions apply](#).

You may also be interested in:

[Gas/oil/water flow measurement by electrical capacitance tomography](#)

Yi Li, Wuqiang Yang, Cheng-gang Xie et al.

[Three-phase flow measurement in the petroleum industry](#)

R Thorn, G A Johansen and B T Hjertaker

[Oil–water two-phase flow measurement with combined ultrasonic transducer and electrical sensors](#)

Chao Tan, Ye Yuan, Xiaoxiao Dong et al.

[Real-time model-based image reconstruction with a prior calculated database for electrical capacitance tomography](#)

Marco A Rodriguez Frias and Wuqiang Yang

[Boolean logic analysis for flow regime recognition of gas-liquid horizontal flow](#)

Nicholas P Ramskill and Mi Wang

[Pressure drop, flow pattern and local water volume fraction measurements of oil–water flow in pipes](#)

W A S Kumara, B M Halvorsen and M C Melaaen

[An on-line adaptive estimation method for water holdup measurement in oil–water two-phase flow with a conductance/capacitance sensor](#)

Hao Wu, Chao Tan and Feng Dong

[Modification to mass flow rate correlation in oil–water two-phase flow](#)

Chao Tan and Feng Dong

Experimental measurement of oil–water two-phase flow by data fusion of electrical tomography sensors and venturi tube

Yinyan Liu^{1,2}, Yuchi Deng^{1,2}, Maomao Zhang¹, Peining Yu¹ and Yi Li^{1,3}

¹ Graduate School at Shenzhen, Tsinghua University, Shenzhen 518055, People's Republic of China

² Department of Automation, Tsinghua University, Beijing 100084, People's Republic of China

E-mail: liyi@sz.tsinghua.edu.cn

Received 7 March 2017, revised 11 June 2017

Accepted for publication 15 June 2017

Published 2 August 2017



Abstract

Oil–water two-phase flows are commonly found in the production processes of the petroleum industry. Accurate online measurement of flow rates is crucial to ensure the safety and efficiency of oil exploration and production. A research team from Tsinghua University has developed an experimental apparatus for multiphase flow measurement based on an electrical capacitance tomography (ECT) sensor, an electrical resistance tomography (ERT) sensor, and a venturi tube. This work presents the phase fraction and flow rate measurements of oil–water two-phase flows based on the developed apparatus. Full-range phase fraction can be obtained by the combination of the ECT sensor and the ERT sensor. By data fusion of differential pressures measured by venturi tube and the phase fraction, the total flow rate and single-phase flow rate can be calculated. Dynamic experiments were conducted on the multiphase flow loop in horizontal and vertical pipelines and at various flow rates.

Keywords: electrical capacitance tomography, electrical resistance tomography, oil–water two-phase flow measurement, data fusion

(Some figures may appear in colour only in the online journal)

1. Introduction

It is well known that the oil–water two-phase flow is found widely in the production processes of the petroleum industry. Online measurements of flow parameters such as phase fraction and flow rate of each individual phase, without separating the mixture, are crucial in ensuring the safety and efficiency of oil exploration and production [1]. In contrast to single-phase flow, an oil–water two-phase mixture with the rheological complexity of the coupling effect of oil and water presents different flow regimes. The flow patterns are determined by the flow rate of each individual phase, the viscosity and the density of oil and water, the pressure, and the orientation and geometry of the pipe [2]. Therefore, accurate measurements of key parameters of oil–water flow are always a significant challenge owing to its complex flow behavior.

The oil–water flow, of two immiscible liquids in a pipe, will present complicated flow behavior mainly caused by the large momentum transfer capacity, small buoyancy effects, and low free energy at the interface [3]. The phase inversion of the flow even makes the measurement more complicated, i.e. when the phase fraction reaches certain critical values, the continuous and dispersed phase of flow gradually inverts [4]. In addition, the inclination of the pipe affects the flow regimes, which includes vertical and horizontal flow conditions. Since water is denser than oil, the oil–water two-phase flow presents a major difference between horizontal and vertical conditions due to the effect of gravitational forces. In horizontal pipes, gravity intends to pull the denser phase, i.e. water, down to the bottom of the pipe, which results in completely different flow patterns from the vertical condition [5, 6]. In this work, the effects of different flow rates on measurements in horizontal and vertical pipeline are investigated.

Significant progress has been made in recent years to develop reliable multiphase flow measurement techniques,

³ Author to whom any correspondence should be addressed.

among which a combination of different measuring tools is widely used to obtain information on phase flow rate [7–9]. It is common to find differential pressure (DP) flow meters (such as venturi tubes, orifice plates, cone meters, etc) associated with other kinds of meters, such as void fraction sensors [10–12]. DP flow meters, which are widely used in single-phase flow metering, measure flow rate based on pressure drops produced by the constriction of the tube. They have the advantages of high accuracy and low cost. In this work, the venturi tube is chosen because it has the least influence on flow regimes, the smallest pressure loss, and favorable repeatability compared to other DP meters [8]. However, in multiphase flow measurements, the relationship between the flow rate and the pressure drop across the venturi meter is more complicated than for single-phase flow. To determine the volume flow rates of oil and water flows respectively, the phase fraction (e.g. the water-to-liquid ratio, or WLR) is needed.

A number of techniques have been proposed to calculate phase fractions of multiphase mixtures, such as quick closing valves (QCV), radiation methods, microwave methods and electrical methods, etc. QCV is suitable for steady-state measurements with the advantages of low cost, simple operation and reliability [13]. However, it is an off-line method and limited by non-continuous measurement. Radiation methods including α -ray, x-ray, γ -ray and so on are widely used and are nonintrusive and highly accurate. But since the attenuation coefficients of oil and water are very close, radiation methods have low detection sensitivity [14]. Microwave methods, measuring the holdup based on the different permittivity between oil and water phases, are sensitive to noise and high-cost [15]. Electrical methods have been widely applied in various industrial process applications for real-time measurement because of their low cost, speed, and simplicity. The passive electrical properties of oil and water differ, water being normally of higher permittivity and conductivity than oil. Therefore, oil–water mixtures of different phase fractions have different electrical impedances. Further, electrical tomography technology is applied to visualize the flow regimes via image reconstruction [16].

The electrical measurements studied in this paper consist of capacitive and resistive measurements. As it is known that oil–water two-phase flow can be classified into either of two types, oil-continuous or water-continuous, where the continuous phase has the higher fraction and is dominant within the pipe. For water-continuous flow, the conductive water forms an electrical conductive path between the transmitter and receiver, and distorts the capacitance measurements, where the measured resistance expresses the water content with a much higher accuracy than capacitive measurement. For oil-continuous flow, the major part of the flow is oil, so the resistance measurement is not able to express the ratio of the two phases, as the conductivity within the water has a minor impact on the capacitance measurement. In reality, none of the heterogeneous systems is an ‘ideal dielectric’ or ‘ideal conductor’, and the physical properties of multiphase flow cannot be described by either permittivity or conductivity.

In this paper, two common electrical tomography techniques, electrical capacitance tomography (ECT) and electrical

resistance tomography (ERT) were chosen to measure the phase fraction, to improve measurement accuracy and extend the measurement range [17, 18]. ECT is suitable for measuring water holdup of oil-continuous flows through capacitance measurement, since oil–water mixtures with varying water holdups have varying dielectric properties. And ERT is used to calculate the phase fraction of water-continuous multiphase flows, so phase fractions from 0% to 100% can be derived.

The present work focuses on the measurement of flow rate and phase fraction of oil–water flows. Experiments in horizontal and vertical pipes with various flow rates were conducted to calculate the WLR and the flow rate of oil–water flows. The complex behavior of oil–water mixtures under different conditions was also analyzed by image reconstruction. Since the mechanical pumping used to lift oil to ground level in the process of oil exploration could generate periodical pulses of gas–oil–water mixtures, pulse experiments were also conducted to investigate the effect on accuracy measurement of oil–water flows.

2. Methodology

2.1. Electrical measurement

2.1.1. Sensor principle. ECT provides a non-intrusive way to visualize the permittivity distribution of dielectric materials by measuring the changes in capacitance over the electrode pairs. Generally, an ECT system is composed of three main components: an ECT sensor, a data acquisition system, and a computer. The capacitance data from the sensor array is transferred to the data acquisition system to be processed and displayed on the computer. A typical ECT sensor consists of 8 electrodes evenly installed on the external surface of an insulating pipe [19]. Each electrode can be configured to act as a transmitter or a detector. For an N -electrode ECT system, when one of the electrodes is excited in turn and the other electrodes are kept at zero potential, the number of independent capacitance measurements will be $N(N - 1)/2$ [20].

In ECT, the boundary conditions are the electrical potential distribution $\phi = V$ for excited electrodes and $\phi = 0$ for rest electrodes. In 2D geometry, the relationship between the capacitance and the permittivity distribution can be expressed as [20]:

$$C = \frac{Q}{V} = -\frac{1}{V} \iint_{\Gamma} \varepsilon(x, y) \nabla \phi(x, y) d\Gamma \quad (1)$$

where Q is the electric charge, $\varepsilon(x, y)$ and $\phi(x, y)$ are the permittivity distribution and the potential distribution respectively in the sensing area, Γ is the electrode surface and ∇ represents a gradient operator.

Similar to ECT systems, an ERT system also has as its main components a sensor, a data acquisition system and a PC. An ERT sensor measuring conductivity distribution relies on current injection into the fluid via electrodes set in the pipe wall. Thus, unlike the non-invasive ECT sensor, it must be in direct electrical contact with the flow inside the pipe [21]. When a

pair of adjacent electrodes is selected for current injection, the voltage between all the other combinations of neighbor electrodes is measured. Subsequently the next pair of electrodes is selected, followed by all the others [21]. The total number of measurements for an N -electrode ERT sensor is $N(N - 3)/2$. An 8-electrode system yields 20 independent measurements.

For ERT, the relationship between the conductance and the conductivity distribution can be expressed by the following equation [17]:

$$G = \frac{I}{V} = -\frac{1}{V} \int \int_{\Gamma} \sigma(x, y) \nabla \phi(x, y) d\Gamma \quad (2)$$

where $\sigma(x, y)$ is the spatial conductivity distribution in the sensing area and V is the potential difference between the receiver electrodes.

2.1.2. Calculation of WLR. Before the quantification of a water-to-liquid ratio (WLR), appropriate calibration strategies should be applied on raw measurements (capacitance for ECT and voltage for ERT) to minimize the impact of noise due to the screen, the pipe wall and the cables. Normally a high calibration point is needed for ECT measurements [2]. However, it is difficult to obtain in a real-time process in actual industry application due to the limitation of the ECT measurement. Thus, in this work, the raw capacitance measurements of ECT are normalized based only on a low calibration point C_1 (such as full-pipe oil with relative permittivity $\varepsilon_1 = \varepsilon_{\text{oil}} = 2.2$), which is easily obtained. The further data analysis is processed based on this low-calibration normalized capacitance measurement. Similarly, the raw voltage measurements of ERT are normalized by a low calibration point V_w (e.g. full-pipe water with relative permittivity $\varepsilon_{\text{water}} = 78$, and conductivity $\sigma_{\text{water}} = 270 \mu\text{s cm}^{-1}$) only:

$$\begin{aligned} C_n &= \frac{C_m - C_1}{C_1} \\ V_n &= \frac{V_m - V_w}{V_w} \end{aligned} \quad (3)$$

where C_n and V_n are the normalized capacitance and voltage respectively, and C_m and V_m are the measured raw capacitance and voltage from ECT and ERT of different flow distributions respectively.

Theoretically, the equivalent capacitance C_x of fluid can be assumed to be proportional to permittivity ε_x and equivalent voltage V_x is inversely proportional to conductivity σ_x , namely:

$$\begin{aligned} C_x &\propto \varepsilon_x \\ V_x &\propto 1/\sigma_x. \end{aligned} \quad (4)$$

Thus from equations (3) and (4), the relative permittivity ε_m and conductivity σ_m of the oil–water mixture flow can be calculated from C_n and V_n respectively:

$$\begin{aligned} \varepsilon_m &= (C_n + 1)\varepsilon_1 \\ \sigma_m &= \sigma_w / (V_n + 1). \end{aligned} \quad (5)$$

The relative permittivity and conductivity of oil- and water-continuous mixtures can be converted to phase fractions using Ramu-Rao's model [15]:

$$\begin{aligned} \alpha_w &= \frac{\varepsilon_m - \varepsilon_{\text{oil}}}{\varepsilon_m + \chi\varepsilon_{\text{oil}}} \\ \alpha_w &= \frac{3\sigma_m}{\sigma_m + 2\sigma_{\text{water}}} \end{aligned} \quad (6)$$

where α_w represents the WLR of the oil–water mixture and χ is the empirical coefficient for the oil-continuous flow measurements. It is related to the direction of the pipeline, the geometry of the ECT sensor and also the total volume flow rate Q_l . Based on the ECT sensor and data acquisition system used in this work, χ ranges from 0.2 to 1.0 for horizontal flows and from 0.01 to 0.4 for vertical flows.

Equations (5) and (6) imply that in either oil- or water-continuous oil–water flow, full-range water fraction can be quantitatively calculated from the data fusion of ECT capacitance measurements and ERT voltage measurements.

2.1.3. Quantitative image reconstruction. Since multiphase flow is known as a complex system and highly problematic due to the existence of various flow patterns, non-intrusive visualization of phase distribution inside the pipe is necessary to illustrate the behavior of the oil–water mixture and to understand better the measurement accuracy. With suitable image reconstruction algorithms (e.g. LBP, Landweber, Tikhonov methods and so on [22]), ECT and ERT systems can visualize the electrical property parameter distributions in the cross-section of a pipe.

For a dielectric medium, ECT can be used to reconstruct the permittivity distribution from capacitance measurements [23]. For the conductive medium, ERT is suitable to obtain the conductivity distribution from voltage measurements [24].

Typical ECT/ERT reconstructed image results, i.e. using standard capacitance/voltage measurements, can be seen only as the presence of different materials instead of a distinct distribution of permittivity or conductivity. Thus, in this case, the calculated permittivity ε_m and conductivity σ_m (rather than capacitance and voltage) are used as the input of the image reconstruction algorithm in this work. And the color value of the reconstructed image not only implies the distinction between different materials but also corresponds to the permittivity or conductivity of the mixture.

Linear back projection (LBP), which is widely applied to online image reconstruction because of its simplicity, is used to obtain the quantitative image reconstruction of the oil–water mixture with the calculated ε_m and σ_m , which are obtained by equation (5):

$$g = \frac{S^T \eta}{S^T \mu_\lambda} \quad (7)$$

where g is the reconstructed quantitative image, η is the calculated ε_m or σ_m , S is the normalized sensitivity matrix of ECT or ERT, and μ_λ is the identity vector, i.e. $\mu_\lambda = [1, 1, 1, \dots, 1]^T$. $S^T \mu_\lambda$ is the corresponding change in permittivity when the sensor is first filled with a lower permittivity material and then with a higher permittivity material [22]. The division of $S^T \mu_\lambda$ also makes the center area of the pipeline more sensitive to the capacitance change.

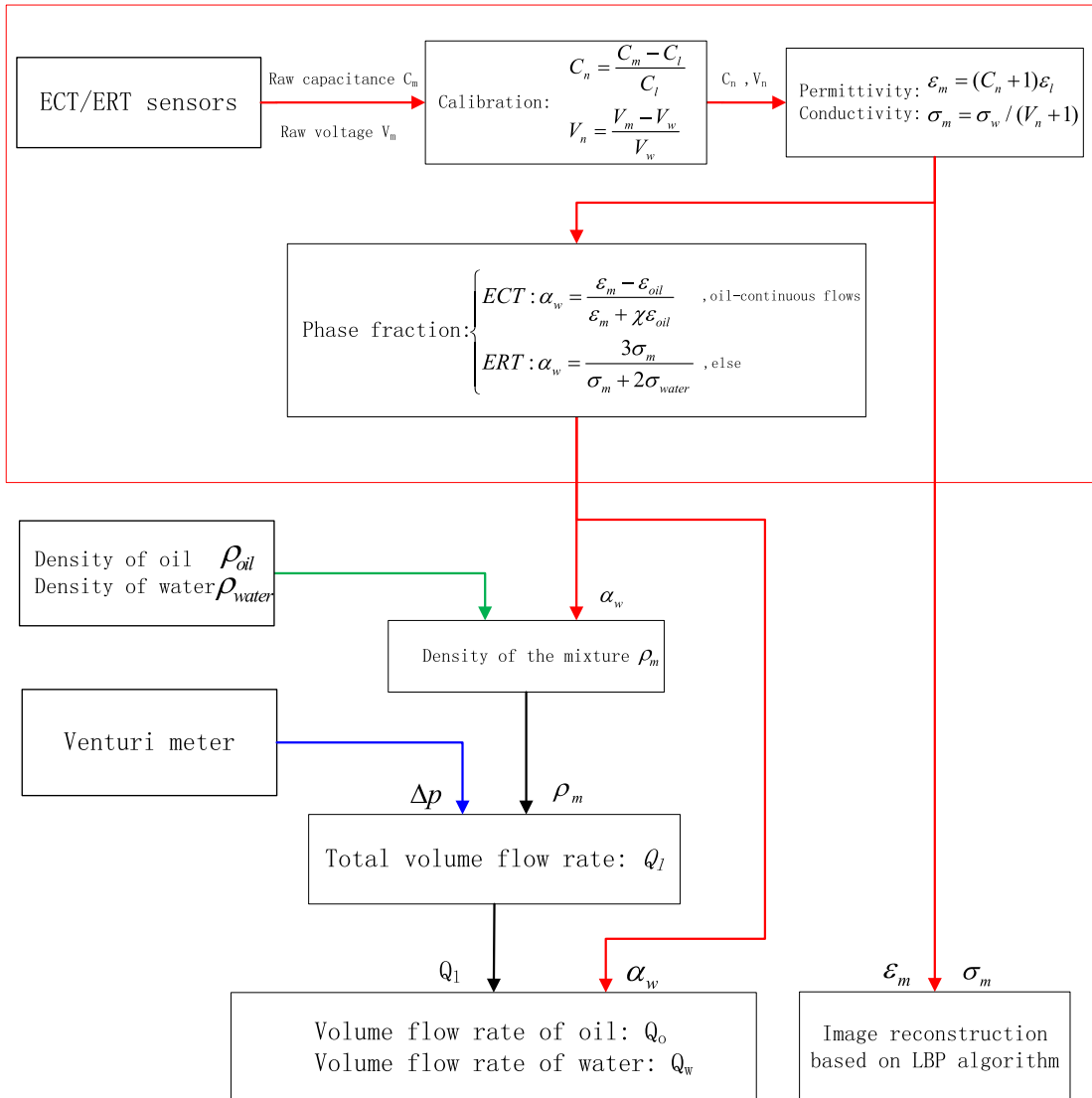


Figure 1. Process of oil–water two-phase flow measurement based on multi-sensor data fusion.

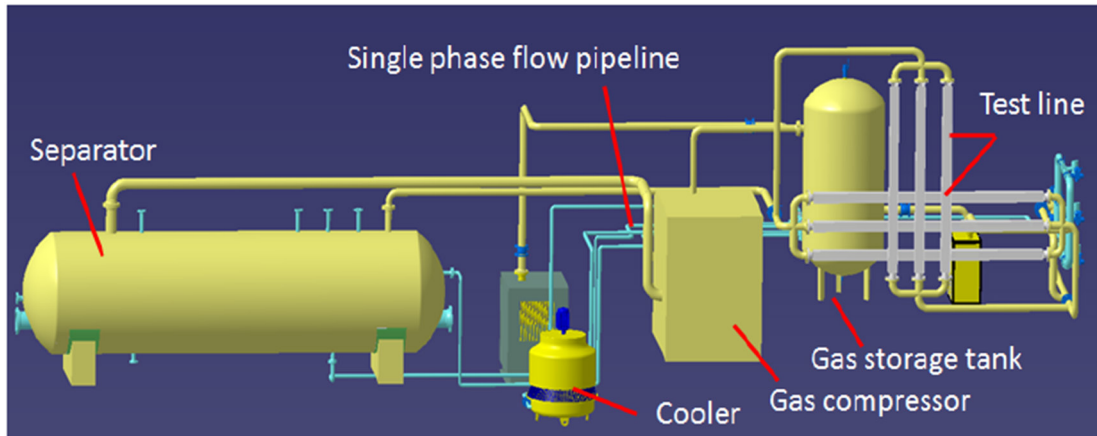


Figure 2. Scheme of gas–oil–water flow facility.

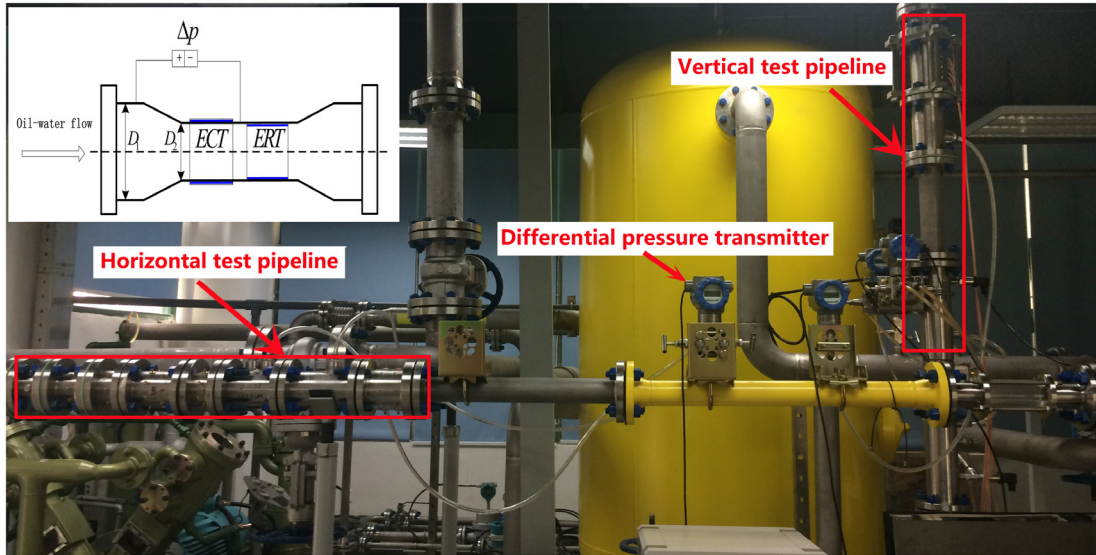


Figure 3. Test section of horizontal and vertical pipeline.

Table 1. Summary of experimental conditions.

Index	Pipe direction	Total flow rate ($\text{m}^3 \text{ h}^{-1}$)	WLR (%)	Measurement step (%)	P (Kpa)	T ($^{\circ}\text{C}$)
H1	Horizontal	10	0–100	10	300	32
H2	Horizontal	20	0–100	5	300	32
H3	Horizontal	25	0–100	5	300	32
V1	Vertical	10	0–100	10	300	32
V2	Vertical	20	0–100	5	300	32
V3	Vertical	25	0–100	5	300	32

2.2. Venturi tube

A venturi tube is basically designed to be used in a single-phase flow. At the throat, the pressure decreases to a minimum where the velocity increases to a maximum since the flow area is decreased. The correlation of volume flow rate Q_l and pressure drop Δp (the differential pressure between the upstream pressure and the throat pressure) is given by [25]:

$$Q_l = \frac{ZYA}{\sqrt{1 - \beta^4}} \sqrt{\frac{2\Delta p}{\rho_m}} \quad (8)$$

where Z is the venturi discharge coefficient, Y is the compressibility coefficient of fluid, for oil–water two-phase flow, and Y is considered to be a constant value of 1. A is the area of the venturi throat, β is the throat-to-pipe diameter ratio and ρ_m is the density of the mixture.

Since the oil–water two-phase flow is more easily homogenized than a gas–liquid mixture, it is usually treated as a pseudo-homogeneous flow, i.e. an approximate single phase, thus equation (8) can be applied directly. The mixture density of oil–water flow can be calculated by oil density ρ_{oil} , water density ρ_{water} and the phase fraction α_w :

Table 2. Summary of pulse experimental conditions.

Index	Pipe direction	Total flow rate ($\text{m}^3 \text{ h}^{-1}$)	WLR (%)	P (Kpa)	T ($^{\circ}\text{C}$)
1	Horizontal	10	10/20/40/80	300	32
2	Horizontal	20	10/20/40/80	300	32
3	Vertical	10	10/20/40/80	300	32
4	Vertical	20	10/20/40/80	300	32

$$\rho_m = \alpha_w \rho_{\text{water}} + (1 - \alpha_w) \rho_{\text{oil}}. \quad (9)$$

The total volume flow rate of oil–water two-phase flow can be derived from differential pressure Δp obtained by venturi tube. Then phase fraction calculated results are used to derive the flow rate of each single fraction:

$$Q_o = \alpha_w Q_l$$

$$Q_w = Q_l - Q_o = (1 - \alpha_w) Q_l \quad (10)$$

where Q_o is oil flow rate and Q_w is water flow rate. In the oil-continuous case, α_w is obtained from the ECT measurement, and in the water-continuous case, α_w is calculated from the ERT measurement.

2.3. Multi-sensor data fusion

In accordance with the above analysis, the process of oil–water two-phase flow measurement by combining an ECT sensor, an ERT sensor and a venturi tube is described in figure 1. The electrical sensors are used to calculate the full-range phase fraction of the oil–water flows. By the data fusion of phase fraction, single-phase density and the differential pressure obtained by venturi tube, the total volume flow rate of oil–water two-phase flow can be measured. The phase flow rate measurement can be achieved from the total volume flow rate and the phase fraction.

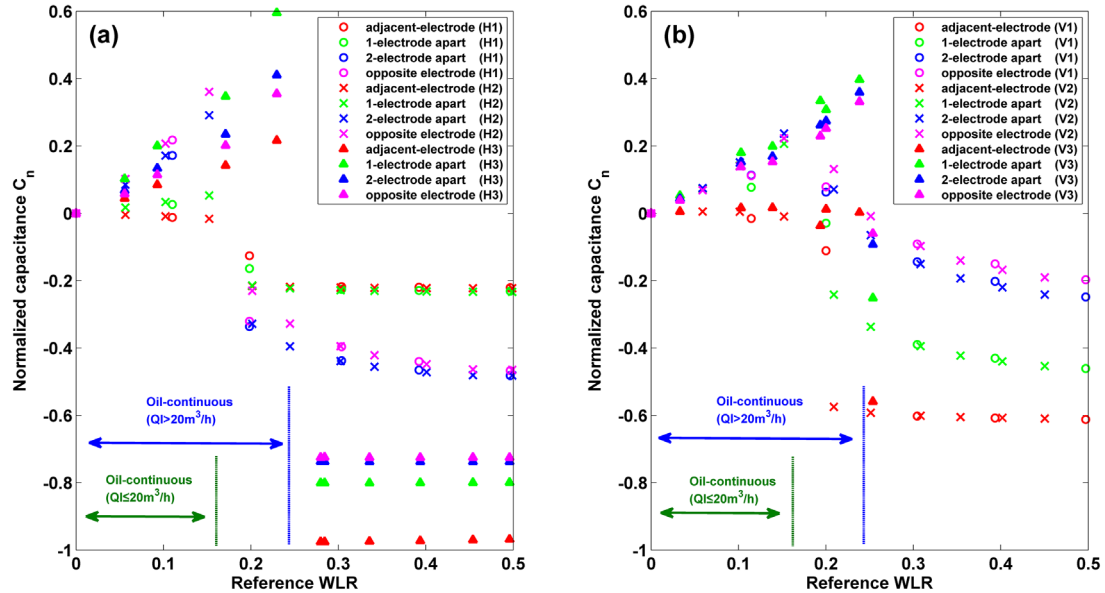


Figure 4. ECT normalized capacitance based on time-average results: (a) horizontal flow measurements; (b) vertical flow measurements.

3. Experimental set-up

3.1. Facility

The experiments were carried out in the semi-industrial standard gas–oil–water multiphase flow facility in the Graduate School at Shenzhen, Tsinghua University. As described in figure 2, oil and water stored in the separator can be simply separated based on the gravity principle. The pipelines shown in blue represent the single phases of gas, oil and water. Oil and water are pumped from the separator and the gas phase will be generated from a gas compressor. Thus, a three-phase mixture can pass through the horizontal or vertical test line (in gray, in sizes of 2, 3 or 4 inches). The design length of the test line is 8 m. Different sensor sections, ECT or ERT, can be located on the test line. The maximum flow rate of an oil–water mixture is $35 \text{ m}^3 \text{ h}^{-1}$. The maximum pressure that the facility can hold is 2 Mpa.

In this work, ECT and ERT sensors were located on the venturi throat section (see figure 3). An ECT sensor of 8 electrodes was installed outside a 5 mm thick insulating pipe liner made from PEEK (relative dielectric constant $\epsilon_r \approx 3.2$). An ERT sensor with 8 electrodes was installed on the inner surface of the pipe wall. The axial length of the sensors is 60 mm, and each electrode is 30 mm long. An AC-based data acquisition system is used to take measurements from the ECT and ERT sensors [26]. The data sampling rate are about 300 frames s^{-1} , 120 frames s^{-1} and 4 frames s^{-1} for the ECT system, ERT system and venturi tube, respectively. The excitation signal frequency is 100 kHz for the ECT system and 20 kHz for the ERT system. The signal-to-noise ratio of the hardware system is around 62 dB.

3.2. Experimental conditions

Both horizontal and vertical flows were tested, at different flow rates. The experimental materials were technical white

oil with relative permittivity $\epsilon_{\text{oil}} = 2.2$, density $\rho_{\text{oil}} = 880 \text{ kg m}^{-3}$ and viscosity $\mu_{\text{oil}} = 8.8 \text{ mPa} \cdot \text{s}$ (32°C), and local tap water of conductivity $\sigma_{\text{water}} = 270 \mu\text{s cm}^{-1}$ and density $\rho_{\text{water}} = 998 \text{ kg m}^{-3}$. The working pressure is set to 0.3 Mpa. The temperature of the flows is about 32°C , which is obtained by a temperature transmitter. The total flow rate of oil–water flow was fixed in several values through our experiments: 10, 20, and $25 \text{ m}^3 \text{ h}^{-1}$. Then with the fixed total flow rate, the ratio between the water and oil was adjusted to reach varying water fractions, i.e. the WLR for measurements. Experimental measurements were not taken until the single flow rates were stabilized and the mixing process of the two fluids was completed. The sampling time for each test point was 30–60 s. The experimental conditions are summarized in table 1. To simulate the mechanical pumping process during the artificial lifting of oil to ground level in the process of oil exploration, pulse experiments were also conducted to estimate the accuracy measurement of the discontinuous varying oil–water flow (see table 2).

4. Results and discussion

4.1. Data analysis

In accordance with the number of intervening electrodes separated between an excited electrode and a measured electrode, the 28 capacitance measurements of the 8-electrode ECT sensor used in this work can be classified into four independent groups: ‘adjacent-electrode’, ‘one-electrode apart’, ‘two-electrodes apart’ and ‘opposite-electrode’ (say cross-pipe) measurements [27]. To reduce the inhomogeneity of oil–water flow, ‘adjacent-electrode’, ‘one-electrode apart’, ‘two-electrodes apart’ and ‘opposite-electrode’ of 8-, 8-, 8- and 4-view spatial averages are conducted. Figure 4 shows the time-average (about 10 s) normalized capacitance measurements of different measurement groups with varying WLR of horizontal and vertical flows. Note that for oil-continuous flow, with the increase of WLR, the normalized capacitances

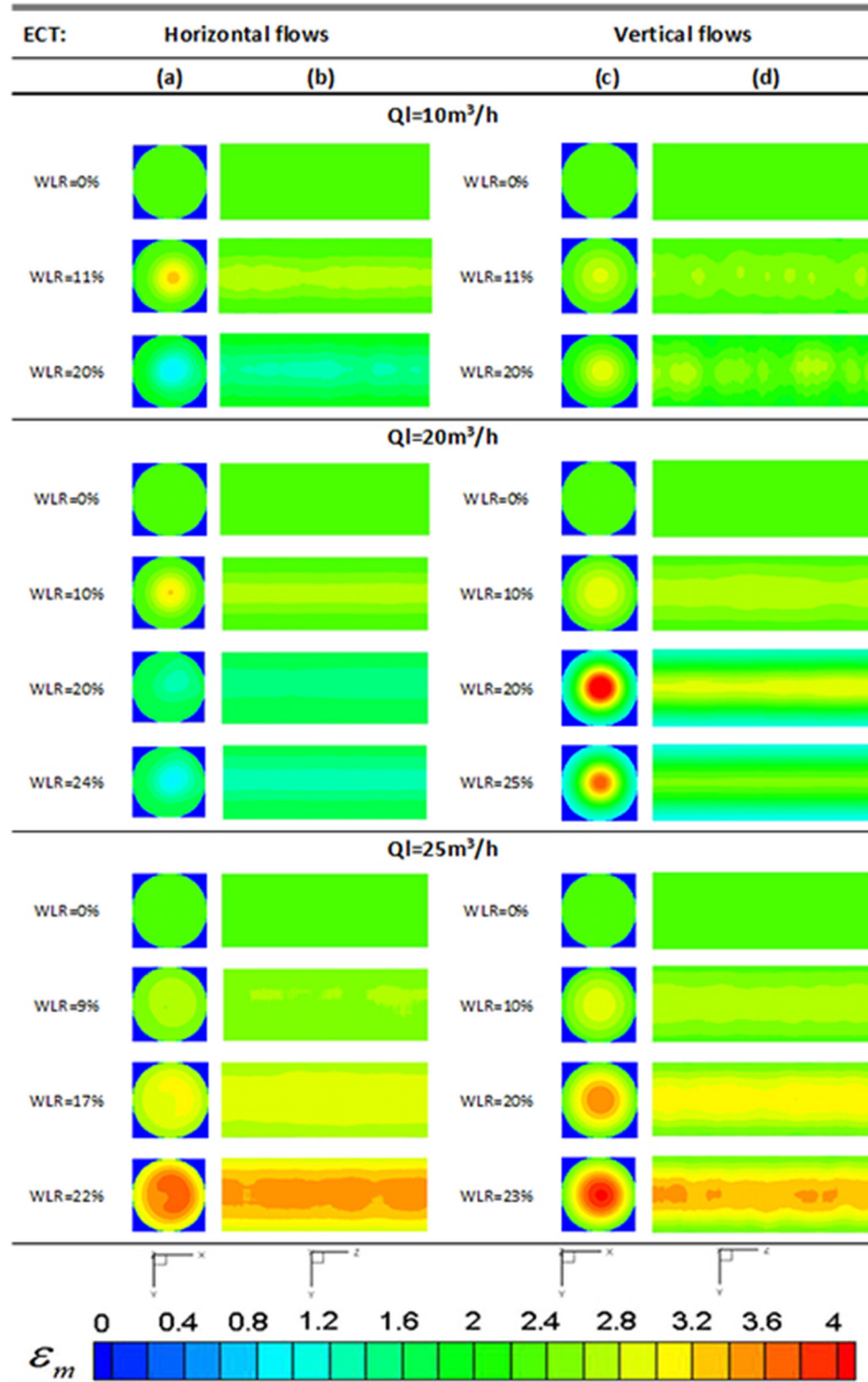


Figure 5. Time-average ($\sim 4\text{ s}$, total 1000 frames) ECT cross-sectional and instantaneous longitudinal images of horizontal/vertical flows with different flow rates based on LBP. (a) Time-average cross-sectional images of horizontal flows (permittivity-change colour scale shown at bottom). (b) Instantaneous longitudinal images of horizontal flows. (c) Time-average cross-sectional images of vertical flows. (d) Instantaneous longitudinal images of vertical flows.

increase approximately linearly. A peak value is encountered when the water phase fraction reaches a critical point, where phase inversion is assumed to take place. For a low flow rate (say $Q_l \leq 20\text{ m}^3\text{ h}^{-1}$), phase inversion occurs when WLR is below 20%, while it appears at about 25% for a high flow rate

(say $Q_l = 25\text{ m}^3\text{ h}^{-1}$). This illustrates that phase inversion is related to flow rate: the higher the flow rate, the more homogeneous the mixture. It should be emphasized again that the conversion point could differ for different oils, as it depends on the degree of homogeneity of the oil and water mixture.

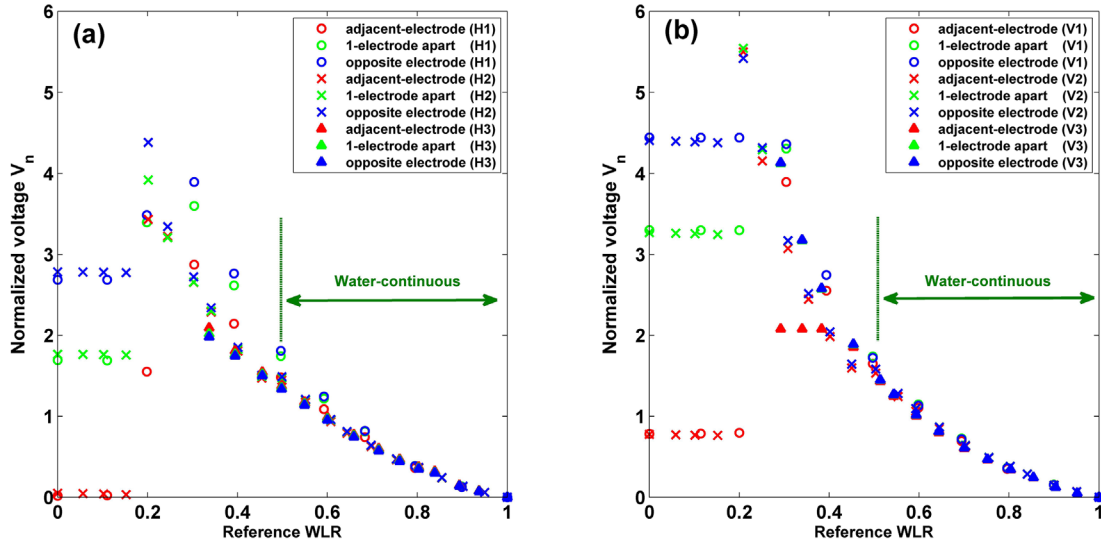


Figure 6. ERT normalized voltage based on $\sim 10\text{s}$ time-average results: (a) horizontal flow measurements; (b) vertical flow measurements.

After reaching the phase inversion point, a further increase in WLR may cause intermittent phase inversion because of water agglomeration, and finally forms water-continuous flow. During the transition from oil-continuous flow to water-continuous flow, the ECT sensor may still work, despite the normalized capacitance decrease with the increase of WLR (see figure 4). Since oil and water do not mix well, the normalized capacitances become negative in value. A core-annular flow pattern was observed from ECT image reconstruction, with the oil phase encircled by a layer of water in the pipes (see figure 5). When a mixture becomes completely water-continuous, a short-circuiting effect of the conductive water will occur. The ECT system loses efficiency for capacitance measurement and the normalized capacitance reaches a constant value even if the water fraction increases [28].

As shown in figure 4, the ‘adjacent-electrode’ measurement results are insensitive to the water phase fraction in oil-continuous flows, since the sensitive region of adjacent electrodes is a small area close to the two electrodes, and the outermost layer of fluid is the oil phase with high viscosity and which clings to the inner pipe wall, so the variation of the flow in the central region has only a small impact on these measurements. This can also be validated by the reconstructed images shown in figure 5. The normalized capacitances of the other three measurement groups are sensitive and proportional to the water phase fraction before the phase inversion point, which means that the more water flows, the larger the capacitance of the mixture will be for the oil-continuous flow. The ‘one-electrode apart’ (near-wall region), ‘two-electrodes apart’ (near cross-pipe region) and ‘opposite-electrode’ (cross-pipe region) measurements can reflect the oil–water mixture changes in the whole pipe, since their sensing region covers a larger area than that of the ‘adjacent-electrode’ measurements. Compared with horizontal flows (see figure 4(a)), it is found that oil and water are better mixed in vertical flows (see figure 4(b)). This is probably due to the horizontal flows suffering from the effect of gravitational forces (see columns (a) and (b) in figure 5).

For the 8-electrode ERT sensor used in this paper, when current is applied through two neighboring electrodes, voltage measurements can be obtained from successive pairs of neighboring electrodes, one-electrode apart electrodes and diametrically opposed electrodes, so the total voltage measurements can be classified into three independent groups: ‘adjacent-electrode’ and ‘one-electrode apart’ and ‘opposite-electrode’ measurements. Figure 6 shows that the normalized voltages vary with the WLRs of horizontal and vertical flows in different experimental conditions. It indicates that the normalized voltages are almost constant when the WLR is less than 20% since the conductive path will break when the water fraction is too low, which conforms that an ERT system is suitable for measuring continuous flows with conductivity, i.e. oil is dispersed in a water-continuous flow. The normalized voltage decreases with an increase of water fraction when WLR is more than 20%. According to equation (5), because water conductivity is higher than oil conductivity ($\sigma_{\text{oil}} = 0 \text{ ms cm}^{-1}$), as WLR increases, the mixture conductivity increases and measured voltage decreases. For horizontal flows (see figure 6(a)), there was no significant difference in normalized voltage among the three groups for the mixture with $10 \text{ m}^3 \text{ h}^{-1}$ flow rates when WLR was greater than 50%, but the normalized voltage V_n varies widely when WLR becomes smaller, say 20%–40%, since the flow is in the transition region. For $20 \text{ m}^3 \text{ h}^{-1}$ flows, V_n decreases with an increase of WLR when WLR is more than 20%, and has a good agreement between the three groups when the water fraction is more than 25%. This is probably because the oil–water flow is well mixed at a higher flow rate. For vertical oil–water two-phase flows (see figure 6(b)), there are some abnormal points for flows at $Q_l = 25 \text{ m}^3 \text{ h}^{-1}$, where the difference among three groups is great, with the WLR = 20%–40%. It is possible that rotational flow distribution occurs at a high flow rate, resulting in a separated liquid–liquid layer.

Figure 7 shows the quantitative LBP reconstruction image using average measurements and frame-by-frame measurements of ERT for both horizontal and vertical flows. It indicates that conductivity increases with increasing WLR. With

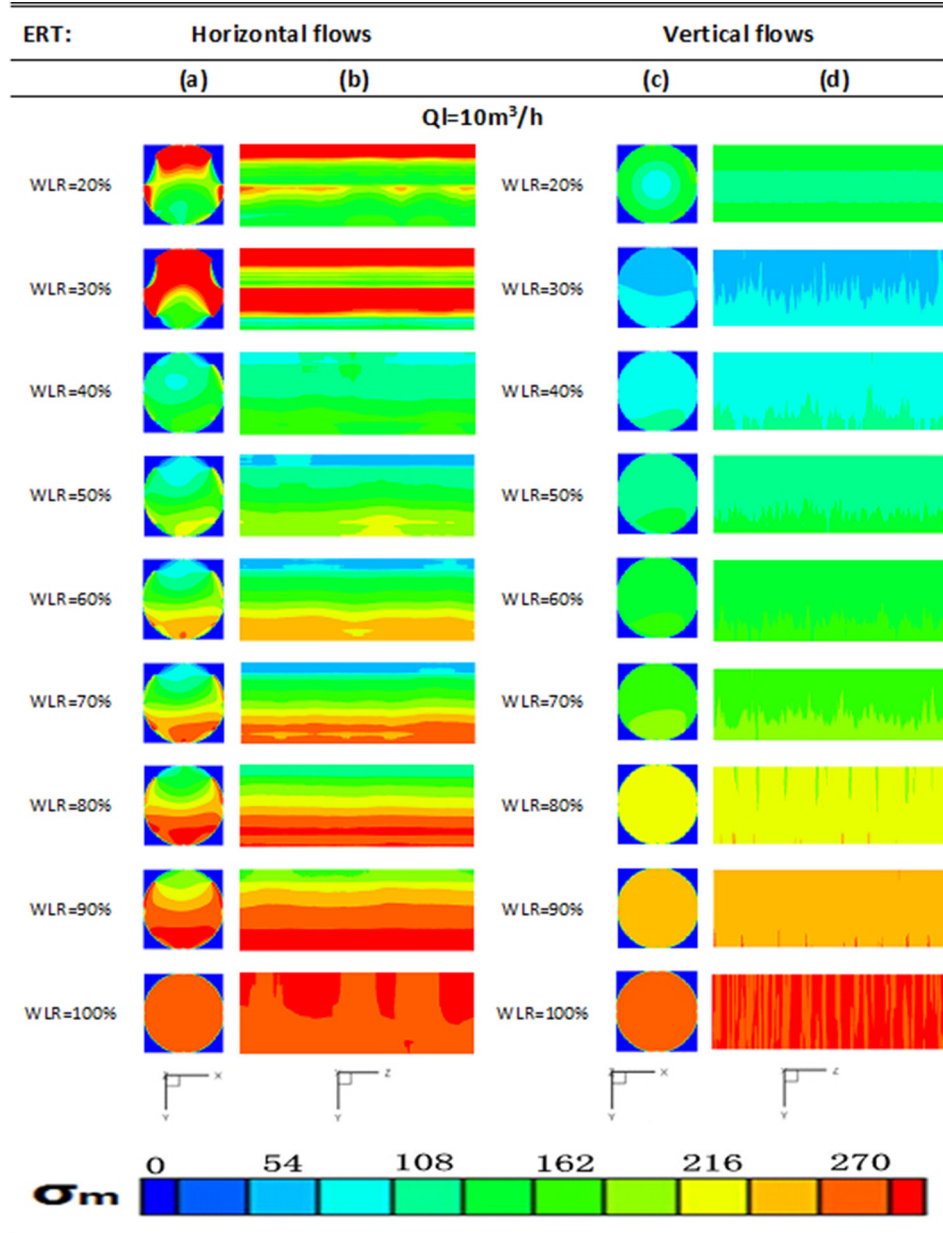


Figure 7. Time-average (~ 8 s, total 1000 frames) ERT cross-sectional and instantaneous longitudinal images of horizontal and vertical flows with total flow rate $Q_1 = 10 \text{ m}^3 \text{ h}^{-1}$ based on LBP. (a) Time-average cross-sectional images of horizontal flows (conductivity-change colour scale shown at bottom). (b) Instantaneous longitudinal images of horizontal flows. (c) Time-average cross-sectional images of vertical flows. (d) Instantaneous longitudinal images of vertical flows.

the reconstructed conductivity distribution derived from real-time measurements, it is helpful to judge whether the mixture is well-mixed or not. For horizontal flows, with the increase of water fraction, the flow distribution becomes stratified, as presented in the images. Since the density of water is higher, most of the water phase stays in the bottom of the pipe due to gravity. However, gravity will not affect the flow significantly for a vertical pipe, thus a more homogeneous oil–water mixture can be obtained (see figures 7(c) and (d)).

Based on the analysis above, ‘one-electrode apart’, ‘two-electrodes apart’ and ‘opposite-electrode’ measurements of ECT are used to calculate the WLR for oil-continuous flows by equation (6). In this work, χ is 0.6 for horizontal flows and 0.2 for vertical flows. ERT is used to measure the water

fraction when the WLR is between 20% and 100%. The choice of ECT or ERT to calculate the phase fraction is mainly based on whether the flow is oil-continuous or not. Figure 4 shows that when the normalized capacitance of adjacent pair measurement is more than -0.1 , the flow is oil-continuous, no matter whether the pipeline is horizontal or vertical. When the normalized capacitance of adjacent pair measurement is less than -0.1 , ERT measurements will be chosen to calculate WLR as ECT already does not work. So, by the data fusion of ECT and ERT measurements, the calculation of full-range WLR for both horizontal and vertical oil–water flows can be obtained. Figure 8 shows the calculated WLR of horizontal flows. It indicates that when the water fraction is less than 20%, the error of measured WLR in different flow rates is

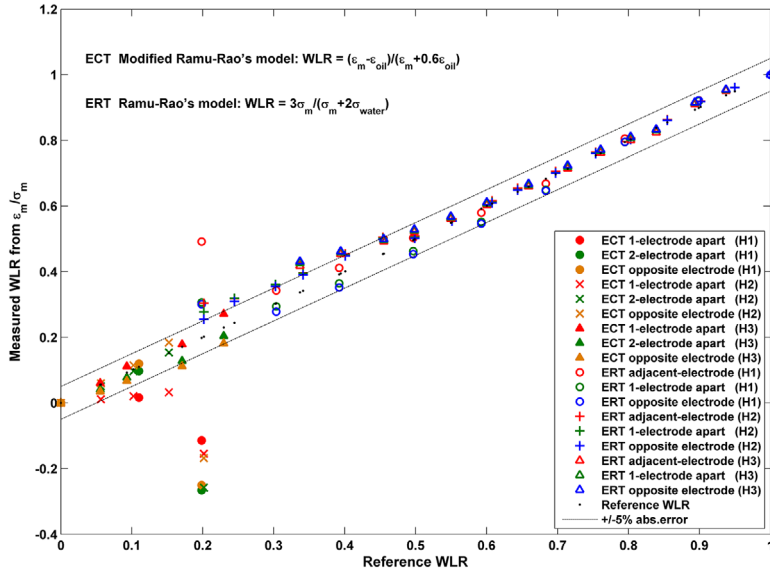


Figure 8. Measured WLR of horizontal flows based on time-average ECT and ERT data.

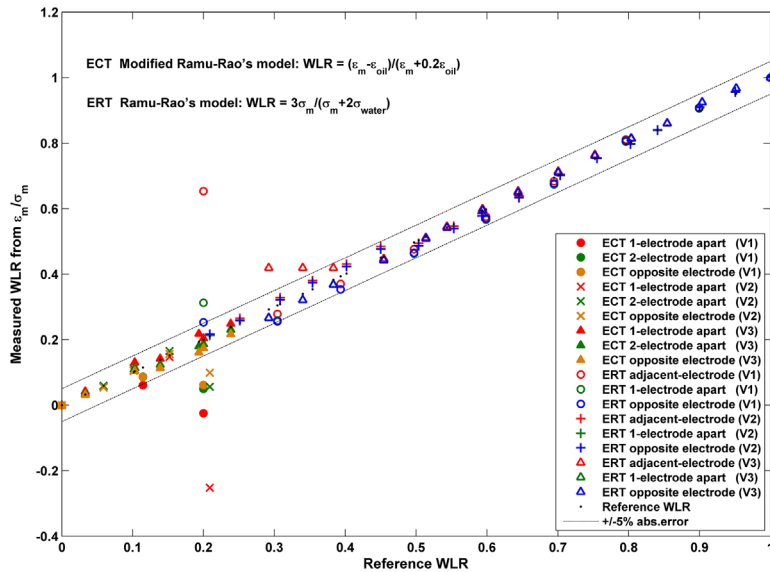


Figure 9. Measured WLR of vertical flows based on time-average ECT and ERT data.

less than 5% with the ‘two-electrodes apart’ and ‘opposite-electrode’ measurements of ECT, while ‘one-electrode apart’ (near-wall region) measurements have a marked underestimation at low flow rates (say $Q_l \leq 20 \text{ m}^3 \text{ h}^{-1}$). At the point where WLR = 20%, neither ECT nor ERT measurement results perform well. For $Q_l = 25 \text{ m}^3 \text{ h}^{-1}$, acceptable results from ECT measurements can be obtained up to WLR = 25%. For ERT results, a significant deviation from reference WLR occurs when WLR is less than 50% (the phase transport region), but the error is still acceptable. The measured WLR from ‘one-electrode apart’ and ‘two-electrodes apart’ measurements are more accurate than that of ‘adjacent-electrode’, since the measurement groups of ‘one-electrode apart’ and ‘two-electrodes apart’ can diminish the effect of ‘assumed’ inhomogeneous flow by spatial average. From WLR = 50% to 100%, the mixture can be regarded as ‘perfect’ water-continuous flow, and the calculated WLRs are all within $\pm 5\%$ absolute error at different flow rates.

Figure 9 shows the vertical flow measurement results calculated by the data fusion of ECT and ERT measurements. With the total flow rate $Q_l = 25 \text{ m}^3 \text{ h}^{-1}$, the absolute error of WLR stays within $\pm 5\%$ for WLR = 0%–100%. And for $Q_l = 20 \text{ m}^3 \text{ h}^{-1}$, the effective measurement region for ECT is WLR = 0%–15%, and WLR = 20%–100% for ERT. For the low flow rate (say $Q_l = 10 \text{ m}^3 \text{ h}^{-1}$), both the ECT and ERT results have a significant deviation when WLR = 20%. Similar to horizontal flows, the error of WLR obtained by ‘two-electrodes apart’ and ‘opposite-electrode’ measurements of ECT is less than $\pm 5\%$ for WLRs up to 15%, and the ‘one-electrode apart’ measurements results are underestimated. For vertical flow with different flow rates, the effective range of ERT is from 20% to 100% and the absolute error is within $\pm 5\%$ based on the measurements of ‘one-electrode apart’ and ‘two-electrodes apart’ measurements. However, the adjacent-pair measurements show increased error during the transition region for the oil–water mixture at a $25 \text{ m}^3 \text{ h}^{-1}$ total flow rate.

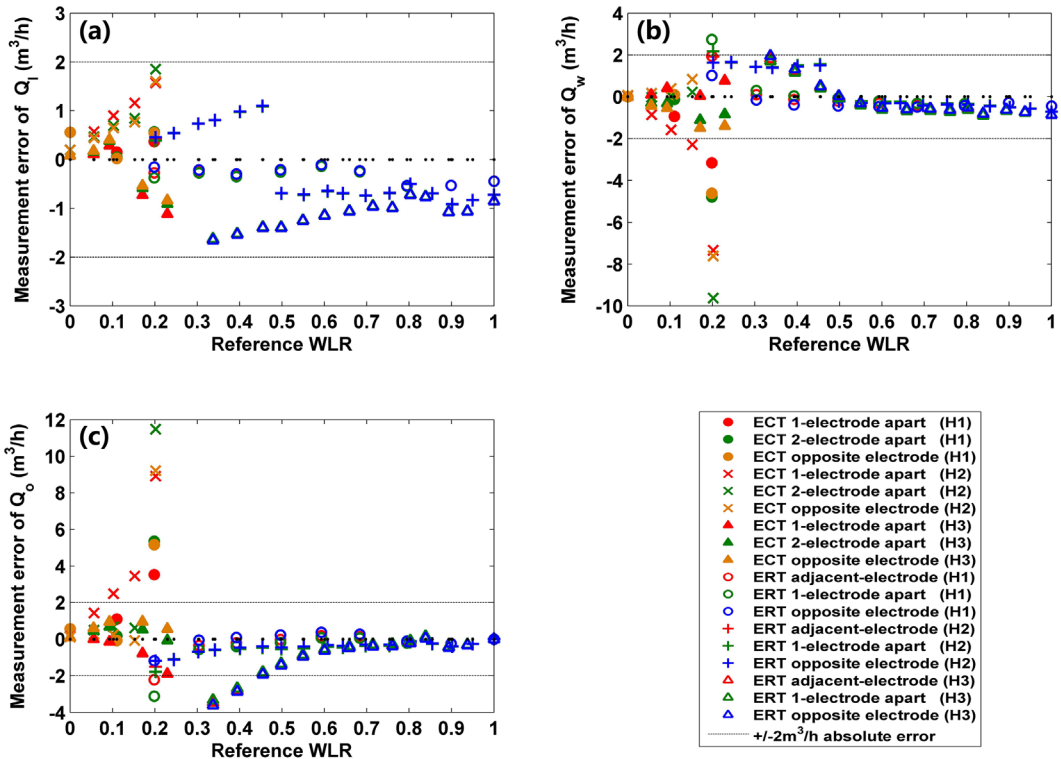


Figure 10. The absolute error in flow rate of horizontal flows by using equation (9) plotted versus reference WLR for: (a) total flow rate; (b) flow rate of water; and (c) flow rate of oil.

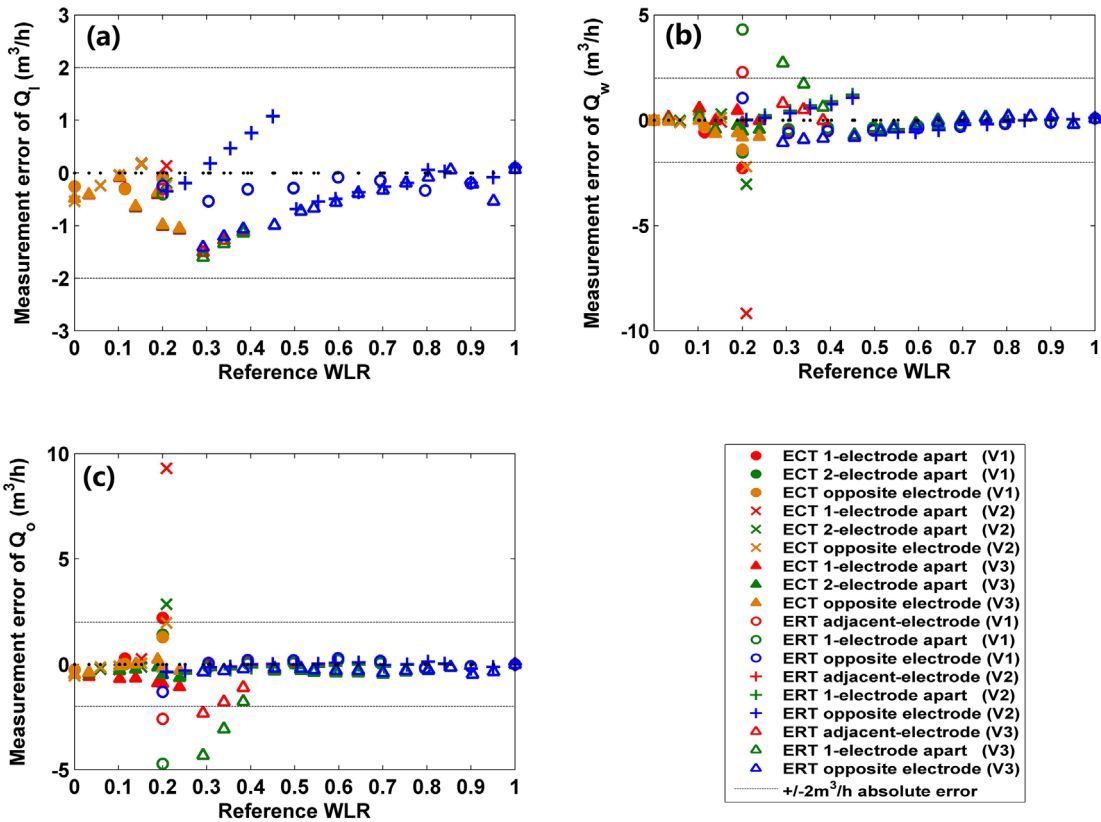


Figure 11. The absolute error in flow rate of vertical flows by using equation (9) plotted versus reference WLR for: (a) total flow rate; (b) flow rate of water; and (c) flow rate of oil.

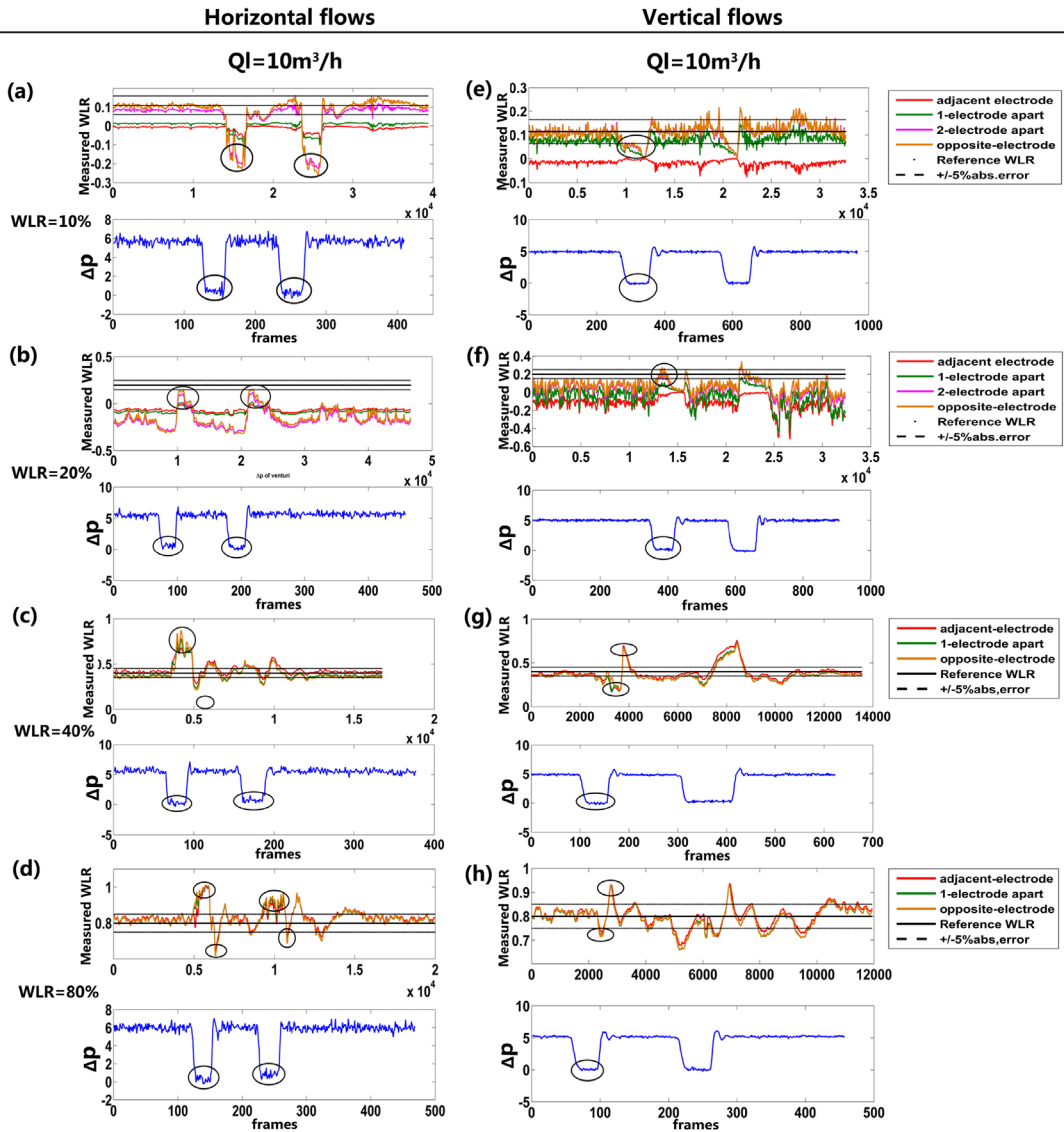


Figure 12. The measured WLR and differential pressure plotted versus frames for pulse experiments in horizontal and vertical conditions, with total flow rate of $10 \text{ m}^3 \text{ h}^{-1}$. For horizontal flows with $Q_l = 10 \text{ m}^3 \text{ h}^{-1}$: (a) WLR = 10%, (b) WLR = 20%, (c) WLR = 40%, (d) WLR = 80%. For vertical flows with $Q_l = 10 \text{ m}^3 \text{ h}^{-1}$: (e) WLR = 10%, (f) WLR = 20%, (g) WLR = 40%, (h) WLR = 80%.

Based on the process shown in figure 1, the phase fraction is integrated with the differential pressure measured from the venturi tube to calculate the total flow rate Q_l and single-phase flow rates Q_o and Q_w . The measurement errors in horizontal and vertical flows are shown in figures 10 and 11 respectively. For both horizontal and vertical flows, the calculated Q_l can be within $\pm 2 \text{ m}^3 \text{ h}^{-1}$ absolute error at different flow rates. During the phase inversion, where WLR ranges from 20% to 50% in this work, the measurement results are overvalued for $Q_l = 20 \text{ m}^3 \text{ h}^{-1}$ and underestimated for $Q_l = 25 \text{ m}^3 \text{ h}^{-1}$. The single-phase flow rates Q_o and Q_w also encounter a significant error around the transition point. Figure 11 shows that the measured WLRs of vertical flows are much more accurate than those of horizontal flows. For both the calculated total and the single-phase flow rate from 'opposite-electrode' measurements, the absolute error can be within $\pm 2 \text{ m}^3 \text{ h}^{-1}$ even though other group measurements ('one-electrode apart' and 'two-electrodes apart' measurements for the ECT sensor

and 'adjacent electrode' and 'one-electrode apart' measurements for the ERT sensor) are inaccurate when WLR = 20%.

Figures 5 and 7 show that the oil–water flow with different flow rates in horizontal and vertical pipelines present different flow patterns. So the future work will focus on calculating WLR based on the flow pattern recognition and giving a comprehensive comparison among the calculated results of different mixing permittivity models, such as Maxwell Garnett formula and Böttcher model.

4.2. Pulse effect

In oil and gas exploration on land, mechanical pumping of production on artificial lift is popular, particularly for those wells on their last period. The mechanical pumping could generate periodical pulses of gas–oil–water mixture, thus the flow rate and water fraction could vary. This scenario is simulated in our lab by using switch on/off valves located before

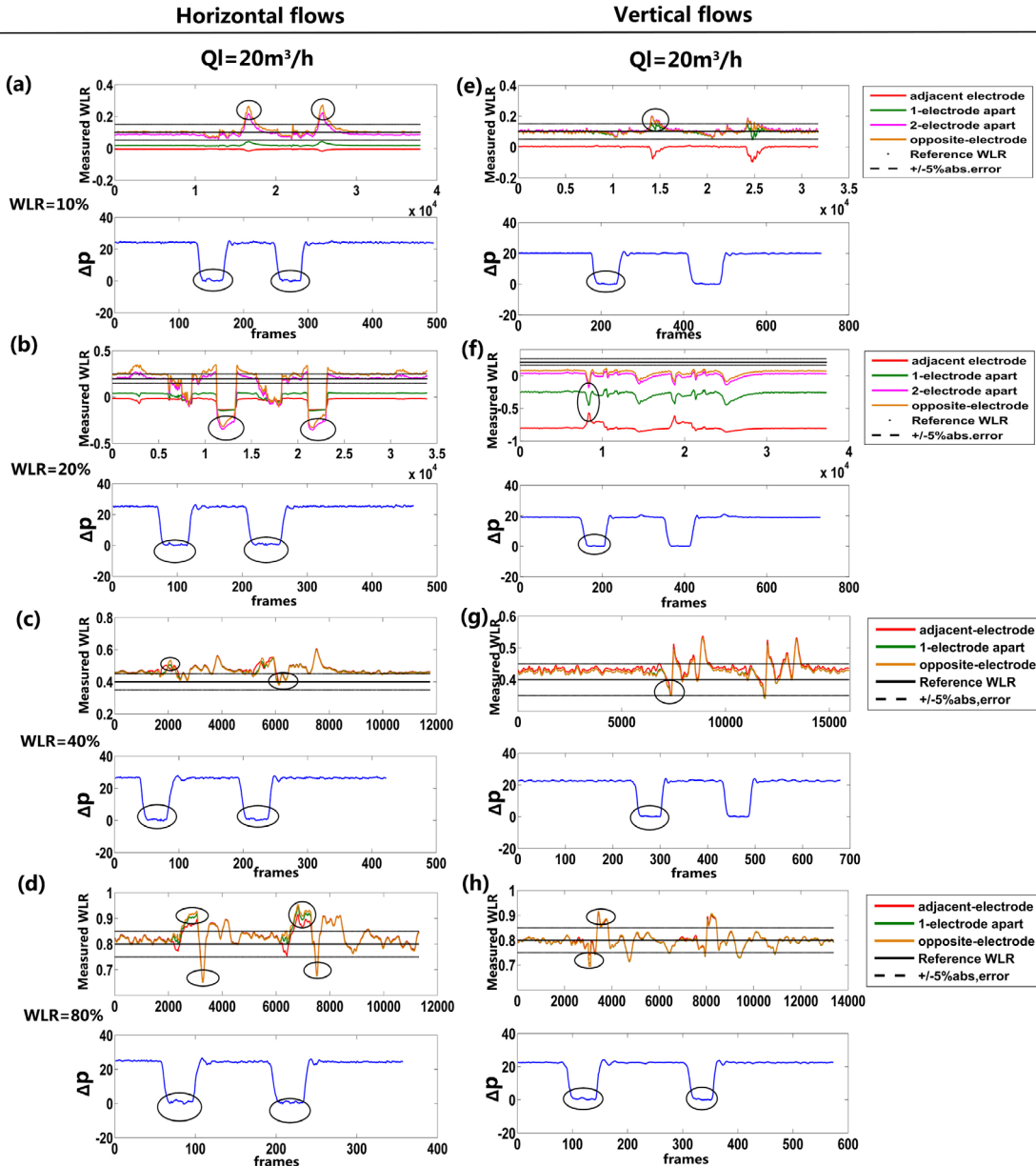


Figure 13. The measured WLR and differential pressure plotted versus frames for pulse experiments in horizontal and vertical conditions, with total flow rate of $20 \text{ m}^3 \text{ h}^{-1}$. For horizontal flows with $Q_l = 20 \text{ m}^3 \text{ h}^{-1}$: (a) WLR = 10%, (b) WLR = 20%, (c) WLR = 40%, (d) WLR = 80%. For vertical flows with $Q_l = 20 \text{ m}^3 \text{ h}^{-1}$: (e) WLR = 10%, (f) WLR = 20%, (g) WLR = 40%, (h) WLR = 80%.

the test pipeline. When the oil–water pulse streams pass through the sensors, the differential pressure Δp obtained by venturi tube declines steeply, as shown in the lower plots (blue line) in figures 12 and 13. The measured Δp shows a sudden large decrease while the valves are switched off. It is believed that the flow rate of the oil–water mixture is seriously fluctuating.

In the measurement of WLR for oil-continuous flows, WLR = 10% and WLR = 20% are measured by the ECT system. ERT is used to measure the mixture with reference WLRs of 40% and 80%; it is complicated in different cases. For the low flow rate, i.e. $Q_l = 10 \text{ m}^3 \text{ h}^{-1}$, and when WLR = 10%, with the decrease of mixture flow rate (valve switches off), the measured water fraction decreases in both horizontal and vertical pipelines (see figures 12(a) and (e)).

However, the ERT measurements show that with a decrease in flow rate of the oil–water mixture, the measured water fraction, e.g. WLR = 40% and 80%, presents a scenario of fluctuation (see figures 12(c), (d), (g) and (h)).

For the flow rate $Q_l = 20 \text{ m}^3 \text{ h}^{-1}$, there is a delay in increasing pulse of measured WLR = 10% while the flow rate of the oil–water mixture decreases (i.e. the valve switches off), as seen in figures 13(a) and (e). By ERT measurement, similar to the $Q_l = 10 \text{ m}^3 \text{ h}^{-1}$ cases, with a decrease in mixture flow rate, the measured water fraction, e.g. WLR = 40% and 80%, fluctuates (see figures 13(c), (d), (g) and (h)).

At this stage, the reasons for this phenomenon have not yet been found, thus the scientific explanation cannot be given. However, it illustrates that production on artificial lift can cause great fluctuations to the phase fraction measurement.

5. Conclusions

This paper investigates the measurements of phase fraction and flow rate of oil–water two-phase flows in both horizontal and vertical pipes by data fusion of ECT and ERT sensors and a venturi tube. ECT is used to measure oil-continuous flow (i.e. WLR < 25%), while ERT is used to calculate WLRs from WLR = 20% to WLR = 100%. The venturi is used to measure the total flow rate of the oil–water mixture. The WLR measured by two measurement groups ('two-electrodes apart' and 'opposite-electrode') of ECT can be kept within a $\pm 5\%$ absolute error before the phase inversion point, say WLR = ~25% for $Q_l = 25 \text{ m}^3 \text{ h}^{-1}$ and WLR = ~20% for $Q_l \leq 20 \text{ m}^3 \text{ h}^{-1}$. But the 'one-electrode apart' (near-wall region) measurements have a marked underestimation of WLR, and the 'adjacent-electrode' measurements are insensitive to WLR variation of oil-continuous flows. Within the range of WLR = 25%–50%, ERT calculation error is more than $\pm 5\%$ for horizontal flows, which are not well mixed due to the effect of gravity, while improved results can be obtained for vertical flows. For the flow of WLR > 50%, the oil–water mixture becomes water-continuous flow, and ERT gives accurate results and maintains the error of WLR within $\pm 5\%$ in both vertical and horizontal pipelines.

The behavior of oil–water two-phase flows is also presented by images reconstruction based on a quantitative LBP algorithm. The results indicate that the phase inversion point is related to the flow rate. The higher the flow rate ($Q_l > 20 \text{ m}^3 \text{ h}^{-1}$ in this work), the more homogeneous the mixture will be, and the phase inversion point will be at a higher WLR. For oil-continuous flows, oil with high viscosity clings to the pipe wall and then a water layer may appear near the wall with the increase of water; this can be visualized from the quantitative image reconstruction. With the increase of water fraction, the flow distribution becomes stratified in horizontal flows due to the effect of gravity, while the oil–water mixture can be more homogeneous in vertical flows.

The total flow rate and single-phase flow rate can be calculated through the data fusion of phase fraction and differential pressure. In either horizontal or vertical conditions, both total flow rate and single-phase flow rate measurements can be within $\pm 2 \text{ m}^3 \text{ h}^{-1}$ absolute error in different flow rate conditions. In the transport region, namely at WLRs ranging from 20% to 50% in this work, the measurement results of Q_w are overvalued and those of Q_o are underestimated for the $20 \text{ m}^3 \text{ h}^{-1}$ and $25 \text{ m}^3 \text{ h}^{-1}$ total flow rates in horizontal flows. Measurement results of vertical flows are more accurate than those of horizontal flows, and both total flow rate and single-phase flow rate measurement results can be within $\pm 2 \text{ m}^3 \text{ h}^{-1}$ absolute error for the full-range WLR with the 'opposite-electrode' measurement data.

The pulse phenomenon always occurs in the artificial lift process, which has much more influence on WLR for horizontal flow compared with vertical flow. The water fraction measurements for oil-continuous flows are underestimated when the total flow rate is small, say $10 \text{ m}^3 \text{ h}^{-1}$, but fluctuate if the flow is in the transport region or is water-continuous. With a total flow rate of $20 \text{ m}^3 \text{ h}^{-1}$, oil-continuous

flows are measured with an overestimated water fraction during the 'pulse period', and the water-continuous flow measurements fluctuate. This illustrates that production on artificial lift can cause great fluctuation of the phase fraction measurement.

Acknowledgments

The authors would like to thank the National Natural Science Foundation of China (No. 61571252, No. 61603207) and the Shenzhen government grant (KQCX20150331151358159) for supporting this work.

References

- [1] Ismail S I et al 2015 Review of oil–water through pipes *Flow Meas. Instrum.* **45** 357–74
- [2] Li Y et al 2013 Gas/oil/water flow measurement by electrical capacitance tomography *Meas. Sci. Technol.* **24** 074001
- [3] Torres C F et al 2016 Oil water flow pattern transition prediction in horizontal pipes *J. Energy Resour. Technol.* **138** 022904
- [4] Brauner N and Maron D M 1992 Flow pattern transitions in two-phase liquid–liquid flow in horizontal tubes *Int. J. Multiph. Flow* **18** 123–40
- [5] Tan C, Wu H and Dong F 2013 Horizontal oil–water two-phase flow measurement with information fusion of conductance ring sensor and cone meter *Flow Meas. Instrum.* **34** 83–90
- [6] Du M et al 2012 Flow pattern and water holdup measurements of vertical upward oil–water two-phase flow in small diameter pipes *Int. J. Multiph. Flow* **41** 91–105
- [7] Tan C et al 2014 A conductance ring coupled cone meter for oil–water two-phase flow measurement *IEEE Sens. J.* **14** 1244–52
- [8] Hasan A 2010 Multiphase flow rate measurement using a novel conductance venturi meter: experimental and theoretical study in different flow regimes *PhD Thesis* University of Huddersfield (<http://eprints.hud.ac.uk/9673/>)
- [9] Li X 2010 Oil–water two-phase flow measurement using a venturi meter and an oval gear flow meter *Chem. Eng. Commun.* **197** 223–1
- [10] Hjertaker B T et al 2005 Multimodality tomography for multiphase hydrocarbon flow measurements *IEEE Sens. J.* **5** 153–60
- [11] Hadžiabdić M and Oliemans R V A 2007 Parametric study of a model for determining the liquid flow-rates from the pressure drop and water hold-up in oil–water flows *Int. J. Multiph. Flow* **33** 1365–94
- [12] Oliveira J L G et al 2009 Mass flow rate measurements in gas–liquid flows by means of a venturi or orifice plate coupled to a void fraction sensor *Exp. Therm. Fluid Sci.* **33** 253–60
- [13] Xue Y et al 2016 Investigation on the void fraction of gas–liquid two-phase flows in vertically-downward pipes *Int. Commun. Heat Mass Transfer* **77** 1–8
- [14] Falcone G, Hewitt G and Alimonti C 2009 *Multiphase Flow Metering: Principles and Applications* (New York: Elsevier)
- [15] Xie C G 2007 Measurement of multiphase flow water fraction and water-cut *AIP Conf. Proc.* **914** 232–9
- [16] Gamio J C et al 2005 Visualisation of gas–oil two-phase flows in pressurised pipes using electrical capacitance tomography *Flow Meas. Instrum.* **16** 129–34
- [17] Li Y and Yang W 2009 Measurement of multi-phase distribution using an integrated dual-modality sensor *IEEE Int. Workshop on Imaging Systems and Techniques* pp 335–9

- [18] Sun J and Yang W 2015 A dual-modality electrical tomography sensor for measurement of gas–oil–water stratified flows *Measurement* **66** 150–60
- [19] Ismail I *et al* 2005 Tomography for multi-phase flow measurement in the oil industry *Flow Meas. Instrum.* **16** 145–55
- [20] Xie C G *et al* 1992 Electrical capacitance tomography for flow imaging: system model for development of image reconstruction algorithms and design of primary sensors *IEEE Proc. G* **139** 89–98
- [21] Dickin F and Wang M 1996 Electrical resistance tomography for process applications *Meas. Sci. Technol.* **7** 247–60
- [22] Yang W Q and Peng L 2003 Image reconstruction algorithms for electrical capacitance tomography *Meas. Sci. Technol.* **14** R1–13
- [23] Zhang M and Soleimani M 2016 Simultaneous reconstruction of permittivity and conductivity using multi-frequency admittance measurement in electrical capacitance tomography *Meas. Sci. Technol.* **27** 025405
- [24] Aw S R *et al* 2014 Electrical resistance tomography: a review of the application of conducting vessel walls *Powder Technol.* **254** 256–64
- [25] Daugherty R L, Finnemore E J and Franzini J B 1997 *Fluid Mechanics with Engineering Applications* (New York: McGraw-Hill) pp 192–8
- [26] Yang W Q and York T A 1999 New AC-based capacitance tomography system *IEEE Proc.* **146** 47–53
- [27] Yang W Q *et al* 2004 Adaptive calibration of a capacitance tomography system for imaging water droplet distribution *Flow Meas. Instrum.* **15** 249–58
- [28] Hammer E A, Tollefsen J and Olsvik K 1989 Capacitance transducers for non-intrusive measurement of water in crude oil *Flow Meas. Instrum.* **1** 51–8